ACS EARTH AND SPACE CHEMISTRY

http://pubs.acs.org/journal/aesccq

Article

Meteorological Influence and Chemical Compositions of Atmospheric Particulate Matters in an Indian Urban Area

Shahadev Rabha, Binoy K Saikia,* Gyanesh Kumar Singh, and Tarun Gupta

Cite This: *ACS Earth Space Chem.* 2021, 5, 1686–1694

Read Online

ACCESS | Metrics & More | Article Recommendations

ABSTRACT: Meteorological conditions essentially impact the emission, distribution, formation, and characteristics of particulate matter (e.g., $PM_{2.5}$) in the atmosphere. In this study, sampling and chemical analysis of $PM_{2.5}$ were carried out for about two winter months during December 2018 and January 2019 to determine their chemical components and possible emission sources in a Northeast Indian urban area (Jorhat). $PM_{2.5}$ mass concentrations were observed to be varied from 81.65 to 193.34 $\mu g\ m^{-3}$ with an average of 117.75 $\mu g\ m^{-3}$, exceeding the permissible limit (60 $\mu g\ m^{-3}$) of the National Ambient Air Quality Standards (NAAQS) of India. The average total water-soluble ions account for 12.27% of total $PM_{2.5}$ mass, of which anions contributed up to 50.52% and cations contributed 49.48%. The correlations among the water-soluble ionic species indicate the formation of NH_4NO_3 and $(NH_4)_2SO_4$ as major ammonium products with high ammonium concentration (30.73% of the total water-soluble aerosol mass) making the $PM_{2.5}$ alkaline. A high concentration of acenaphthylene and naphthalene was also found out of the 16 US EPA poly-aromatic hydrocarbons (PAHs). The correlation study between the chemical components and the meteorological parameters pointed out coal and biomass burning as the main contributor to such high winter loading in Northeast India. Also, the formation of secondary organic carbon up to 21.84 $\mu g\ m^{-3}$ was observed due to suitable meteorological conditions during winter.

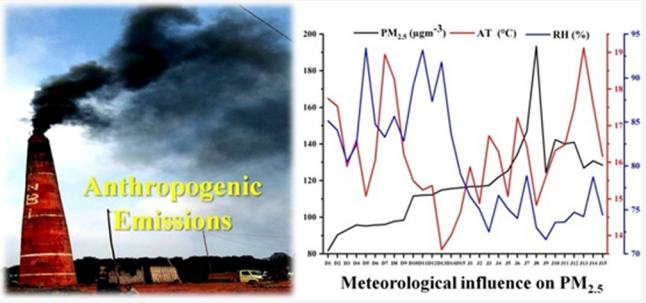

KEYWORDS: *atmospheric aerosols, particulate matter ($PM_{2.5}$), water-soluble ions, PAHs, meteorological impacts, ToF-SIMS*

1. INTRODUCTION

Atmospheric particulate matter impacts global climate systems by influencing the Earth's energy balance and affecting cloud formation.[1,2] Both manmade and natural sources emit particulate matter into the atmosphere. About 90 percent by mass of atmospheric aerosols are natural such as sulfates, sea salt, or ammonium salts, which are the most common cloud condensation nuclei in pristine environments; the remaining 10 percent is emitted from various anthropogenic activities and create great uncertainties in the studies of climate change.[3,4] Anthropogenic aerosols emitted from fossil fuels and biomass burning, such as sulfates, nitrates, and carbonaceous aerosols have both direct and indirect impacts.[5,6] Anthropogenic aerosols dominate in the air downwind of areas with high emission sources having more adverse impacts on local meteorology, air quality, and human health. The impact of meteorology on the $PM_{2.5}$ of chemical compositions differs considerably over time and space depending on their chemical components and on how they affect the particle formation and removal processes.[7] During winter, the aerosol concentration becomes very high due to stable atmospheric conditions, such as subsidence and formation of inversion layers and during the monsoon season; the concentration decreases as the heavy rain wash out particles. In this context, the Northeast regions (NER) of India have special importance due to their unique topography, geographical location, meteorology, and emission sources from increasing anthropogenic activities, which makes the NER a complex aerosol environment. The region is exposed to an annual average greater than 40 $\mu g\ m^{-3}$ of $PM_{2.5}$ pollution.[8] Meanwhile, the $PM_{2.5}$ concentration increases three to four times higher during winter in the region.

A study[10] reported that $PM_{2.5}$ pollution caused about 9156 (95% uncertainty interval) deaths during 2017 in Assam (NER). Jorhat is one of the major growing cities of NER and is located in the middle of the Brahmaputra valley. It experiences significantly higher $PM_{2.5}$ concentrations during winter seasons especially in December–January due to more burning activities and favorable meteorological conditions. Combustion of coal and oils in various anthropogenic activities such as brick kilns,

Received: February 7, 2021
Revised: June 14, 2021
Accepted: June 14, 2021
Published: June 25, 2021

https://doi.org/10.1021/acsearthspacechem.1c00037
ACS Earth Space Chem. 2021, 5, 1686–1694

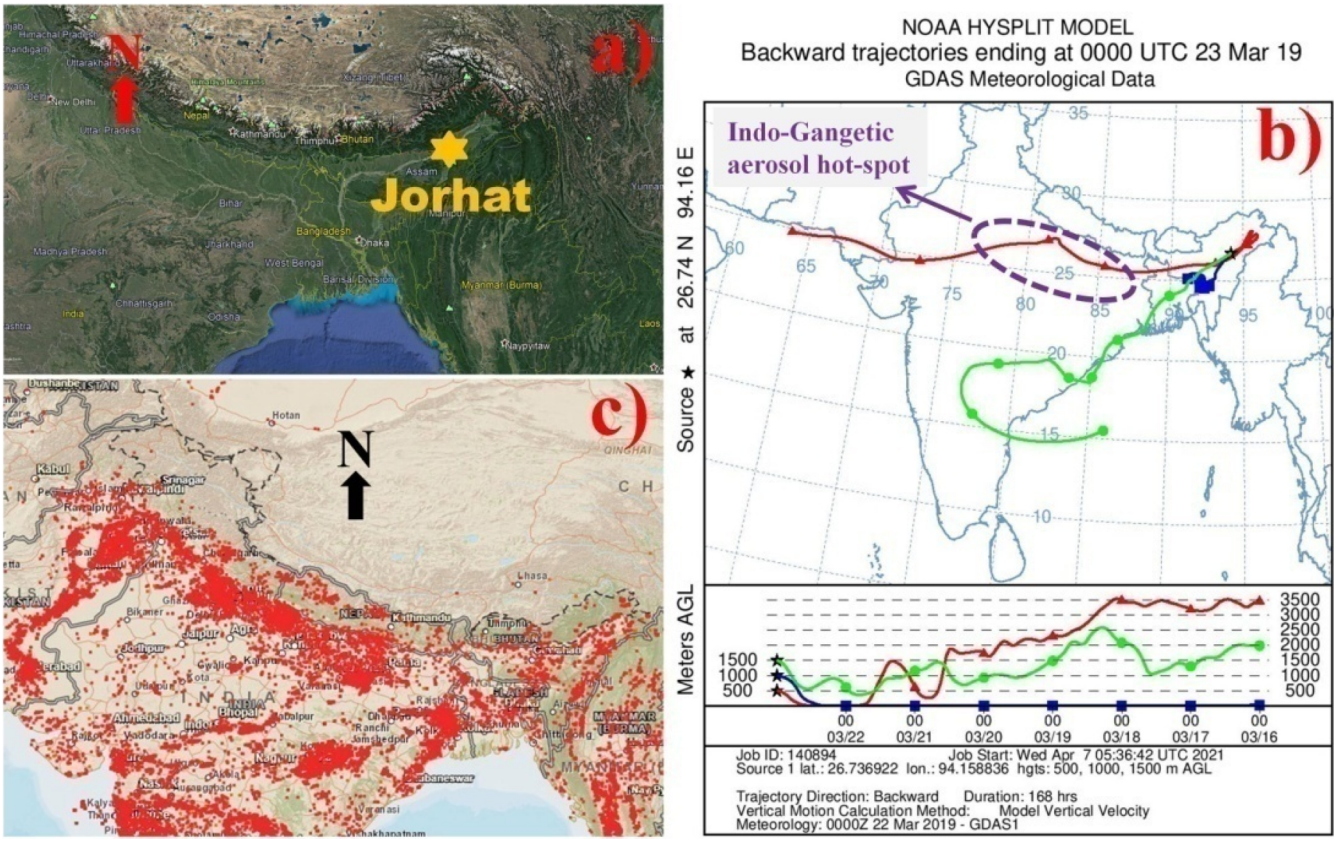

Figure 1. Sampling location: (a) Jorhat city is located at the center of the Brahmaputra valley; (b) seven day back trajectories (representative) reconstructed by the HYSPLIT model for every sampling day showing the long-distance movement of air-masses from the Indo-Gangetic aerosol hot-spot region to the sampling site (red: 500 m AGL, blue: 1000 m AGL, green: 1500 m AGL); (c) fire count map (during December 2018) retrieved from NASA FIRMS showing fire episodes around the sampling site.

cement factories, petroleum oil refineries, tea processing industries, vehicular emissions, and biomass burning in the locality and remote aerosols from the Indo-Gangetic plain, mainland India, west India, and other parts of Asia are the important sources of anthropogenic carbonaceous aerosol in this area.[9−11] Several satellite-based studies were performed in NER India;[11,12] however, proper ground-based observation and physicochemical characterization of the ambient particulate matters and their relationship with local as well as regional meteorology have not been conducted at a significant level. Bhuyan et al.[13,14] studied some of the chemical properties of PM_{10} and source apportionment reporting the contributions from biomass burning, coal burning, petroleum refining, vehicular emission, and crustal dust in this region. Long-range transport and meteorology could also play a major role in the total load of aerosol in the region.[15,16] In the present study, the advanced-level physico-chemical analysis of $PM_{2.5}$ is performed in order to understand the main chemical components during winter high-loading in the Jorhat urban area of NER, and thereby determining the source contributions of these components and the impacts of meteorological conditions.

2. METHODOLOGY

2.1. Sampling Site. The sampling site (26.73 °N, 94.15 °E, elevation of 116 m above mean sea level) is situated about 5 km away from the Jorhat (main commercial/town area) in the west direction. The Jorhat town is located in the center of the Brahmaputra valley of Assam, Northeast India (Figure 1a). The valley experienced a considerable increase in population and various growing developmental activities in recent years,[17] increasing the anthropogenic emission of pollutants. During December−January, various household burning takes place for cooking and heating due to cold weather, and the brick kilns becomes operational, increasing the coal combustion.[18,19] The valley also gets influenced by the air-masses of mainland India and shares the aerosol hot-spot region of the Indo-Gangetic plain during winter.[20] Seven day back trajectories were reconstructed for every sampling day using the Hybrid Single-Particle Lagrangian Integrated Trajectory (HYSPLIT) Model of the NOAA−Air Resource Laboratory at arrival heights of 100, 500, and 1000 m above the ground level to determine the impact of air-masses (Figure 1b). To assess the various burning activities around the sampling site, we retrieved the NASA FIRMS (Fire Information Resource Management System) fire count image from MODIS and VIIRS during aerosol sampling (see Figure 1b). Meteorological data were obtained from an all-in-one (AIO2) automatic weather station (Met One Instruments, USA) located at the sampling site. Meteorological data were collected for 24 h per day at a 1 min resolution every day (1st Dec 2018 to 1st Feb 2019). The 24 h meteorological data were averaged, and sampling day's data were used for the study.

2.2. Sampling of $PM_{2.5}$. A fine particulate matter sampler (Envirotech APM 550) was used to collect $PM_{2.5}$ samples. A total of 60 filter samples were collected (30 Teflon and quartz each) on every alternate day during December 2018 and January 2019 at a height (inlet) of ∼3 m above the ground

https://doi.org/10.1021/acsearthspacechem.1c00037
ACS Earth Space Chem. 2021, 5, 1686−1694

level within the CSIR-NEIST campus. Pre-weighted and pre-treated Teflon (2 μm PTFE 46.2 mm) and Tissuquartz filter (Pallflex 432 μm 47 mm) were used to collect $PM_{2.5}$ samples as reported elsewhere.[21,22] The sampling duration was 24 h for each sample at a 1 m^3 per hour flow rate. The Teflon filters were used to determine the $PM_{2.5}$ mass concentrations, $PM_{2.5}$-bound PAHs and water-soluble inorganic ions, and the Tissuquartz filters were for the mass spectroscopy, electron microscopy, and carbon analysis. The filter samples were wrapped in aluminum foil as specified by the Central Pollution Control Board (CPCB), India, sealed in a Tarson Petri dish and kept in a refrigerator below −4 °C to avoid photo-oxidation and volatilization till further analysis.[22]

2.3. Gravimetric and Chemical Analysis. $PM_{2.5}$ mass concentration was determined gravimetrically by weighing the Teflon filters before and after sampling. The filters were desiccated (20 ± 5 °C and relative humidity 40 ± 2%) for at least 24 h before and after the sampling. The $PM_{2.5}$ mass concentration was calculated from the mass difference of the filters before and after sampling divided by volume of air sampled. The Teflon filter was cut into two equal parts, and one part was extracted using ultrapure water through ultrasonication (Power-Sonic 520) at ambient temperature at a frequency of 40 kHz for 20 min and transferred in the vials using a 0.22 μm Millipore syringe filter to eliminate insoluble parts.[23,24] The filtrates were used for the determination of water-soluble ions using a Metrohm 882 Compact IC Plus system. The water-soluble anions were analyzed by a Metrosep-A Supp 5 (4 mm × 250 mm) analytical column using a mixture of Na_2CO_3 (3.2 mM) and $NaHCO_3$ (1.0 mM) as eluent, and the water-soluble cations were analyzed by a Metrosep-C 4 (4 mm × 150 mm) analytical column using an eluent solution of 0.7 mM dipicolinic acid solution and 0.01% conc. HNO_3 (15.2 N, 67−70% GR grade). Calibration was done by using the standards purchased from Merck.

The other part of the Teflon filter was extracted in toluene using ultrasonic power for 30 min to analyze the $PM_{2.5}$-bound PAHs.[25] The extracts were filtered and concentrated using a rotary evaporator. The impurities in the extract were removed through a silica gel column. A concentrated sample (2 mL) was passed through the column with the subsequent addition of cyclohexane (5 mL) and collected. The extract was evaporated and solvent exchanged with toluene (1 mL) for analysis. Sixteen US-EPA PAHs were measured by the high-performance liquid chromatography (HPLC) technique (Shimadzu HPLC-PDA) using different concentrations of EPA 610 PAH mix-standards (Sigma-Aldrich) for calibration by using the methods reported elsewhere.[26]

The tissuquartz filter was cut into three parts, one part used for the analysis of the surface chemical mass compositions by using time-of-flight secondary ion mass spectroscopy (ToF-SIMS)[27] (Physical Electronics, PHI TRIFT V NANO TOF). The filter samples were cut into 10 mm × 10 mm pieces to insert in the ToF-SIMS sample holder. A control experiment was performed using a blank filter to determine the original composition of blank filters. The second part was used for the analysis of morphological properties by transmission electron microscopy and energy-dispersive X-ray spectroscopy (EDS) (HRTEM: Joel JEM-2100, Japan). Details of transmission electron microscopy were reported elsewhere.[28] The other part of the filter was used to measure the elemental carbon (EC) and organic carbon (OC) concentrations using a DRI (Desert Research Institute) thermo-optical carbon analyzer (model 2015) and IMPROVE (Interagency Monitoring of Protected Visual Environment, 2015) protocol with reflectance charring adjustment.[29] Secondary organic carbon (SOC) in $PM_{2.5}$ was determined by the EC tracer method[30] with eq 1 assuming that the primary OC can be estimated from eq 2:

$$SOC = (OC) - OC_{pri} \quad (1)$$

and

$$OC_{pri} = (EC) \times (OC/EC)_{pri} \quad (2)$$

where $(OC/EC)_{pri}$ denotes the primary OC/EC ratio and (OC) and (EC) are the measured concentrations. The $(OC/EC)_{pri}$ have been estimated from least-square regression (slope = 0.63, intercept = 2.58, and R^2 = 0.61) (Figure 2) on a portion of the data set (23 data points) containing below the threshold (2.12) of the OC/EC ratio, which is comparable with the ratio of 2.22 at the Indo-Gangetic plain (IGP) during winter.[30]

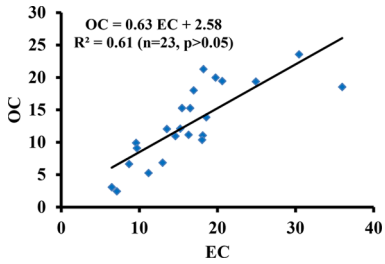

Figure 2. Linear regression of OC with EC to determine the primary OC/EC ratio.

3. RESULTS AND DISCUSSION

3.1. Aerosol Mass Concentration. Aerosol mass concentration is variable and changes with seasons due to seasonal variability of meteorological conditions and anthropogenic emission activities. Meteorological parameters such as temperature and humidity affect the secondary aerosol formation, precipitations help in the wet deposition, and wind effects on aerosol transport and dispersion. During the time of observations, the $PM_{2.5}$ mass concentration varied from 81.65 ± 20.09 $\mu g\ m^{-3}$ to 193.34 ± 59.57 $\mu g\ m^{-3}$ for 24 h sampling with the monthly average of 101.74 ± 10.91 $\mu g\ m^{-3}$ in Dec 2018 and 133.77 ± 19.13 $\mu g\ m^{-3}$ in Jan 2019 (Figure 3). The average $PM_{2.5}$ mass concentration (117.75 ± 22.35 $\mu g\ m^{-3}$) was about two times higher than the permissible limit (60 $\mu g\ m^{-3}$) of the NAAQS in India and about five times higher than the World Health Organisation (WHO) limit (i.e., 25 $\mu g\ m^{-3}$) for a 24 h average in the area. A combination of atmospheric and anthropogenic factors may contribute to this elevated $PM_{2.5}$ pollution during winters such as winter inversion, emissions from combustion of coal in brick kilns and tea industries, open biomass burning, biomass burning for heating and cooking, garbage burning, and formation of secondary aerosols. This elevated $PM_{2.5}$ pollution requires a proper understanding of their characteristics, compositions, and source contributions. Thus, the analysis of various components of this elevated winter $PM_{2.5}$ was carried out by using different analytical techniques and discussed subsequently.

3.2. Water-Soluble Ionic Components. The average total water-soluble ionic components (cations: Na^+, K^+, Ca^{2+},

https://doi.org/10.1021/acsearthspacechem.1c00037
ACS Earth Space Chem. 2021, 5, 1686−1694

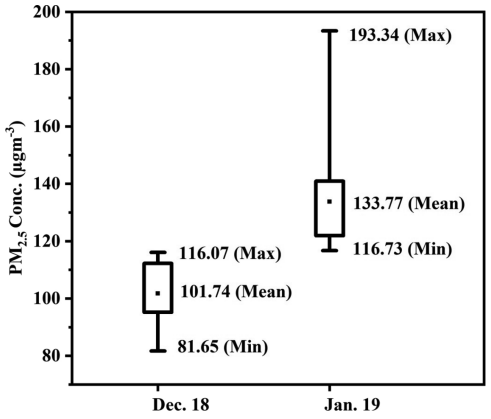

Figure 3. Box whisker plot of $PM_{2.5}$ mass showing the maximum, minimum, and mean (average) concentration $PM_{2.5}$ during sampling periods. The minimum concentration is higher than the permissible limit in India (60 $\mu g\ m^{-3}$).

Mg^{2+}, NH_4^+, and anion: Cl^-, NO_3^-, and SO_4^{2-}) were found to be around 14.45 ± 1.47 $\mu g\ m^{-3}$, which was 12.27% of the $PM_{2.5}$ mass concentration. Table 1 shows the concentrations of water-soluble ions measured during the observation period. The average concentration of anions and cations were in the order of $Cl^- > SO_4^{2-} > NO_3^-$and $NH_4^+ > K^+ > Ca^{2+} > Na^+ > Mg^{2+}$. Among the ionic components, Cl^- contributed the most (31.07%). The contributions of NH_4^+, SO_4^{2-}, and NO_3^- were 30.73, 14, and 5.43%, respectively. The lower concentration of Ca^{2+}, Na^+, and Mg^{2+} may be due to their formation of insoluble carbonates and bicarbonates.

The correlations among the water-soluble ionic species (Table 2) show that NH_4^+ and NO_3^-, NH_4^+, and SO_4^{2-} have a moderate positive correlation (0.33 and 0.25, respectively), indicating the formation of NH_4NO_3 and $(NH_4)_2SO_4$ as major ammonium products. It shows that ammonium has more affinity to the nitrate than sulfate. There are positive correlations of K^+ with Cl^- and NH_4^+ (0.71, 0.44), which might result from the wood biomass burning and coal combustion in the region.[31,32] The good correlations between Ca^{2+} and Mg^{2+} indicate contribution from soil dust, road dust, and construction dust.[33] Na^+, NO_3^-, and SO_4^{2-} mostly related to coal combustion[32] activities around the region. The combustion of Northeastern Indian high-sulfur low-quality coal in the brick kilns and tea industries around the region might be the main reason for high SO_4^{2-} concentration in $PM_{2.5}$.[10] These brick kilns remain active only during the winter season, contributing a significant amount of pollutants within a short period. The frequency of garbage burning and open biomass burning activities also increases during winter, resulting in high Cl^- and NH_4^+ concentrations.[34]

3.2.1. Marine influence on the aerosol compositions. As the study area was located far from marine sources, there were few chances for marine contribution to these water-soluble ionic components. Marine contribution on the aerosol components was generally determined by sea salt ratios by considering that all Na was from the marine origin.[35,36] Table 3 reveals that the aerosol ratios of Cl^-/Na^+, K^+/Na^+, Mg^{2+}/Na^+, Ca^{2+}/Na^+, and SO_4^{2-}/Na^+ were higher than the seawater ratio indicating negligible contribution from the marine source. It confirms that these water-soluble ionic components of aerosol are mostly affected by terrestrial sources from natural or anthropogenic activities.

3.2.2. Acidity of aerosol. The aerosol acidity is generally determined using the equivalent ratios of $NH_4^+/(NO_3^- + SO_4^{2-})$; the ratio greater than or less than one would indicate the alkalinity and acidity, and 1.0 would specify neutralization of H_2SO_4 and HNO_3 by atmospheric NH_3. The observed ratios of $NH_4^+/(NO_3^- + SO_4^{2-})$ were 1.58, indicating the aerosols of weak alkalinity. The alkalinity maybe because of the neutralization of acidity of NO_x and SO_2 by NH_3 emitted from biomass burning, livestock, and agriculture.[37,38]

The anion equivalence and cation equivalence ratio (AE/CE) can be measured to determine the acidity of $PM_{2.5}$, which can be calculated using the equations below[39]

$$AE = \frac{Cl^-}{35.5} + \frac{NO_3^-}{62} + \frac{SO_4^{2-}}{96} \times 2 \quad (3)$$

$$CE = \frac{Na^+}{23} + \frac{NH_4^+}{18} + \frac{Mg^{2+}}{24} \times 2 + \frac{Ca^{2+}}{40} \times 2 + \frac{K^+}{39} \quad (4)$$

The average anion and cation equivalence during the sampling period were 0.18 and 0.35, respectively, and the resultant equivalence ratio was 0.53, which indicates the anion deficiency, resulting in weak alkalinity to $PM_{2.5}$. The anion deficiency may be because of not determining the phosphate (PO_4^{3-}), fluorine (F^-), and carbonate (CO_3^{2-}) ions and volatilization of NO_3^-.

3.3. $PM_{2.5}$-Bound PAHs. PAHs are organic compounds consisting of carbon and hydrogen atoms with at least two fused aromatic ring structures, which releases during fossil fuel combustion and biomass burning.[40,41] Due to their potential toxicity in humans and persistence in the environment, PAHs are of significant environmental concern.[42] Out of 16 US-EPA PAHs determined, eight, including acenaphthene, acenaphthylene, anthracene, benzo(a)anthracene, naphthalene, fluorene, benzo(b)fluoranthene, and pyrene, were found in the sample. Acenaphthylene was found to be the most abounded with 2.60 pg m^{-3} followed by naphthalene (0.79 pg m^{-3}) (Table 4). The obtained PAHs were mostly of low molecular weight (2−3 rings), and the presence of PAHs with high molecular weight (4−5 rings) was very low. The average concentration of $PM_{2.5}$-bound total PAHs was 3.42 ± 0.92 pg m^{-3} during the sampling period. The highly carcinogenic benzo(a)pyrene was below the detection limit in the aerosol samples during the study. The higher concentration of acenaphthylene and naphthalene may be due to an elevated

Table 1. Statistics of Water-Soluble Ion Concentration ($\mu g\ m^{-3}$) between December 2018 and January 2019

species	$PM_{2.5}$ (μgm^{-3})	Cl^-	NO_3^-	SO_4^{2-}	Na^+	NH_4^+	Mg^{2+}	K^+	Ca^{2+}	total ions	total anions	total cations
mean	117.76	4.49	0.78	2.02	0.44	4.44	0.19	1.49	0.58	14.45	7.30	7.15
SD	22.35	0.83	0.41	0.67	0.37	1.66	0.14	0.65	0.30	2.85	1.05	2.20
max	193.35	7.26	2.04	3.58	1.28	8.13	0.50	3.37	1.69	19.28	9.92	10.77
min	81.65	3.35	0.45	0.89	0.00	1.88	0.00	0.37	0.00	7.82	4.76	3.07

https://doi.org/10.1021/acsearthspacechem.1c00037
ACS Earth Space Chem. 2021, 5, 1686−1694

Table 2. Correlations among $PM_{2.5}$ Chemical Components and Meteorological Parameters

parameters ($\mu g\ m^{-3}$)	$PM_{2.5}$	Cl^-	NO_3^-	SO_4^{2-}	Na^+	NH_4^+	Mg^{2+}	K^+	Ca^{2+}	OC	EC	WS ($m\ s^{-1}$)	AT (°C)	RH (%)
$PM_{2.5}$	1													
Cl^-	−0.32	1												
NO_3^-	0.53	−0.26	1											
SO_4^{2-}	0.49	−0.19	0.33	1										
Na^+	0.57	−0.07	0.33	0.39	1									
NH_4^+	0.33	0.11	0.33	0.25	0.19	1								
Mg^{2+}	0.49	−0.22	0.29	0.02	0.31	0.12	1							
K^+	−0.31	0.71	−0.18	−0.14	−0.22	0.44	−0.05	1						
Ca^{2+}	0.03	0.15	−0.08	0.05	0.05	0.11	0.51	0.24	1					
OC	0.92	−0.32	0.52	0.49	0.59	0.27	0.46	−0.30	0.05	1				
EC	0.66	−0.35	0.40	0.27	0.57	0.11	0.37	−0.31	−0.08	0.77	1			
WS ($m\ s^{-1}$)	−0.20	0.00	−0.55	−0.13	−0.20	−0.10	0.04	−0.01	0.01	−0.15	−0.06	1		
AT (°C)	−0.17	−0.03	−0.01	−0.02	−0.19	−0.40	0.02	−0.18	−0.20	−0.21	−0.09	0.03	1	
RH (%)	−0.60	0.31	−0.31	−0.44	−0.47	−0.02	−0.19	0.48	0.24	−0.65	−0.48	0.10	−0.21	1

Table 3. Comparative Ionic Ratios of Aerosols and Seawater

	Cl^-/Na^+	K^+/Na^+	Mg^{2+}/Na^+	Ca^{2+}/Na^+	SO_4^{2-}/Na^+
aerosol	10.20	3.39	0.43	1.32	4.59
seawater	1.80	0.037	0.0119	0.036	0.25

Table 4. Concentrations of $PM_{2.5}$-Bound PAHs

PAHs	pg m^{-3}
naphthalene	0.798
acenaphthylene	2.603
acenaphthene	0.009
anthracene	0.003
fluorene	0.001
pyrene	0.001
benzo(a)anthracene	0.001
benzo(b)fluranthene	0.001
ttotal PAHs	3.41 ± 0.92

amount of coal combustion[40,43] in the brick kilns and household biomass burning in the region.

3.4. OC and EC of the $PM_{2.5}$. The carbonaceous part (i.e., OC and EC) is one of the important constituents of $PM_{2.5}$ resulting from anthropogenic combustion activities. The OC/EC ratios can be used to understand the emission sources and transformation processes of carbonaceous aerosol due to less sensitivity to atmospheric processing.[44,45] An average OC/EC ratio of 2.0 may be attributed to emissions from coal combustion, 1.1 for vehicular emission, and 9.0 for biomass burning.[30,46] The average concentrations of OC were 14.0 ± 7.44 $\mu g\ m^{-3}$, EC was 10.6 ± 7.12 $\mu g\ m^{-3}$, and the OC/EC ratio varies from 0.85 ± 1.74 to 15.44 ± 12.84 with an average of 2.60 ± 3.02, suggesting the emission from biomass burning, vehicles, and coal combustion[22] as the major source of carbonaceous aerosol during winter in the Jorhat area. The correlation between OC and EC (0.77) in $PM_{2.5}$ indicates the emissions of OC and EC in Jorhat area from a similar nature of carbonaceous sources as reported elsewhere.[47]

Secondary organic carbon has significant contribution in altering the OC/EC ratio. The estimated average concentration of SOC was 5.23 ± 4.21 $\mu g\ m^{-3}$, and about 7.84 to 61.861% of the total OC was contributed by SOC. Clear and humid (around 80.29% relative humidity) weather with a high temperature (with a maximum of up to 29.3 °C during daytime) and stable atmosphere (about 0.54 ms^{-1} wind speed) in the area may trigger gas to particle formation resulting SOC formation.[48,49] Further, fossil fuels and biomass combustion results in a higher OC/EC ratio, which can affect the SOC formation by different degrees of atmospheric processing causing overestimation or underestimation of SOC.

3.5. Observations from ToF-SIMS Analysis. ToF-SIMS can provide significant information on the surface chemistry of the aerosols. Figure 4 demonstrates the positive-ion spectra of $PM_{2.5}$ revealing the surface mass chemical compositions. The trace elemental ions detected include Al^+, Ba^+, Ca^+, K^+, Fe^+, S^+, Cd^+, Se^+, Zn^+, Ti^+, and Pb^+. The presence of nitrogenous organic compounds such as NH^+ (m/z 15) and CH_3N^+ (m/z 29) and sulfur-containing compounds such as $C_4H_5S^+$ (m/z 85), $C_4H_6SO_4^+$ (m/z 134), and $C_8H_5S_2^+$ (m/z 165) attributed to the coal combustion and vehicular emissions[27] was detected in the $PM_{2.5}$ samples. ToF-SIMS also indicated the presence of PAHs such as naphthalene (m/z 128) and acenaphthylene (m/z 152); these were also found to be the most abundant individual $PM_{2.5}$-bound PAHs in the samples during PAH analysis by HPLC. The adherence of these inorganic elements and organic components to particles surface signifies the harmfulness of $PM_{2.5}$.[50]

3.6. Observations from HR-TEM Analysis. Observation by transmission electron microscopy mostly reveals minerals, soot particles, and organic matter. The main compositions of the mineral particles, as obtained from EDS, were O, Si, Mg, Na, K, Ca, and Fe. The Ca-rich (Figure 5a) and K-rich (Figure 5b) particles were found as the major minerals, serving as a tracer of coal combustion and biomass burning.[51−53] The Si-rich particles (Figure 5c) associated in the samples commonly serve as a tracer of road dust or crustal emission.[54] Aggregates of soot particles were found extensively in the sample, with a single aggregate containing hundreds of carbon particles (Figure 5d). Soot aggregates were found to be associated with organic matter (Figure 5e). High-resolution TEM of soot particles, originating from the incomplete combustion of fossil fuels and biomass burning, reveals onion-like discontinuous graphitic layers (Figure 6a).[28] Carbon nanostructures containing carbon nanotubes[55] and graphene-like sheets[56] were observed (Figure 6b,c). The selected area electron diffraction (SAED) pattern shows characteristics of the graphene-like sheet[56] (Figure 6d). Such carbon nanostructures could be formed due to the combustion of wood sources (domestic

https://doi.org/10.1021/acsearthspacechem.1c00037
ACS Earth Space Chem. 2021, 5, 1686−1694

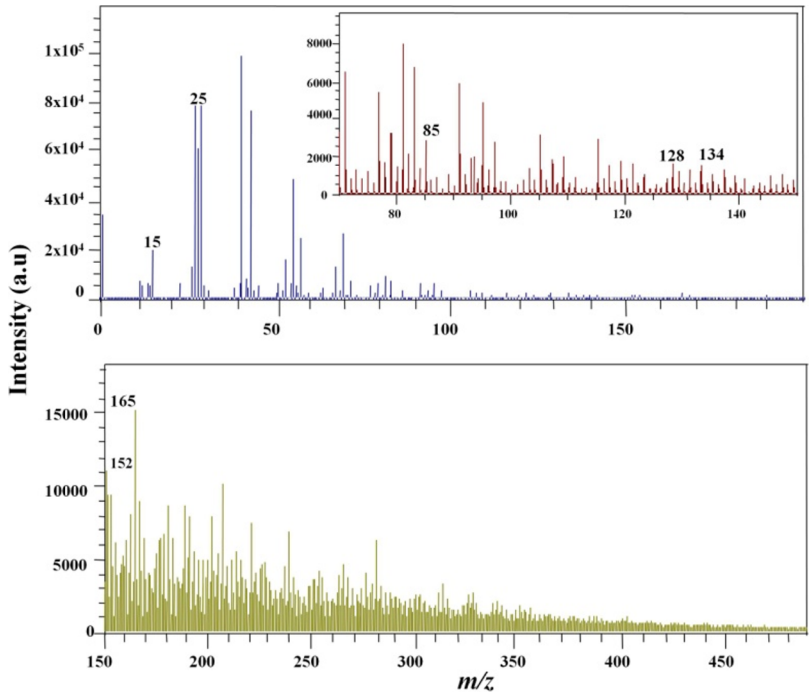

Figure 4. Positive ion ToF-SIM spectra of $PM_{2.5}$ reveal the presence of naphthalene, acenaphthylene, nitrogenous, and sulfur-containing compounds.

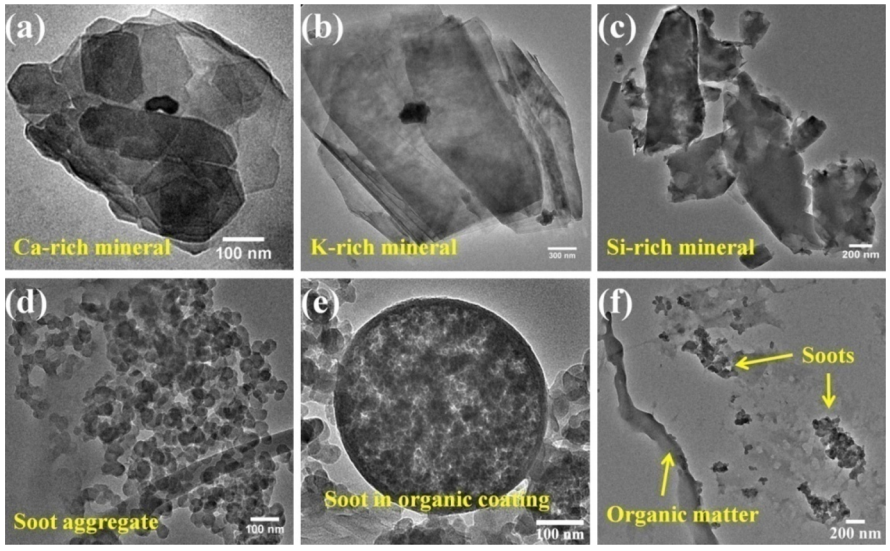

Figure 5. High-resolution transmission electron microscopic images. (a) Mineral rich in calcium, (b) mineral rich in potassium, (c) silicate mineral from road dust, (d) aggregate of soot particles, (e) soot aggregate inside the organic matter coating, and (f) organic matter and soots.

cooking) as well as fossil fuels such as diesel and petrol, which is also reported elsewhere.[56,57]

3.7. Meteorological Implications. The daily-average temperature during the sampling period was 16.22 °C (max 19.12 °C, min 13.62 °C) and daily average relative humidity was 80.29% (max 93.41%, min 71.63%). The daily average wind speed was 0.54 ms^{-1}, and the wind direction was from the southeast direction (Figure 7). Figure 8 shows the variation of $PM_{2.5}$ mass relative to the temperature, and relative humidity. Pearson's correlation matrix (Table 2) demonstrates the relationships between the $PM_{2.5}$ mass and their chemical components with the meteorological parameters during the sampling period. The $PM_{2.5}$ mass shows a negative correlation with the temperature, relative humidity, and wind speed. The chemical components also mostly had a negative correlation except for Mg^{2+}, K^+, and Ca^{2+}. Mg^{2+} shows a positive correlation with temperature and wind speed and K^+ and Ca^{2+} with relative humidity. Temperature, relative humidity, and wind speed play a crucial role in $PM_{2.5}$ concentrations in most regions. High temperature can increase the sulfate concentrations due to oxidation of SO_2 and decrease nitrate levels due to volatilization of ammonium nitrate.[58] The total $PM_{2.5}$ may be dominated by the increase in sulfate or decrease in nitrate. The negative correlation (−0.17) of the average total $PM_{2.5}$ could be due to decreases in nitrate with the increase of temperature. $PM_{2.5}$ has shown a negative correlation (−0.60) with relative humidity during the study period.[59] This could be because the relative humidity was higher at night (average:

https://doi.org/10.1021/acsearthspacechem.1c00037
ACS Earth Space Chem. 2021, 5, 1686−1694

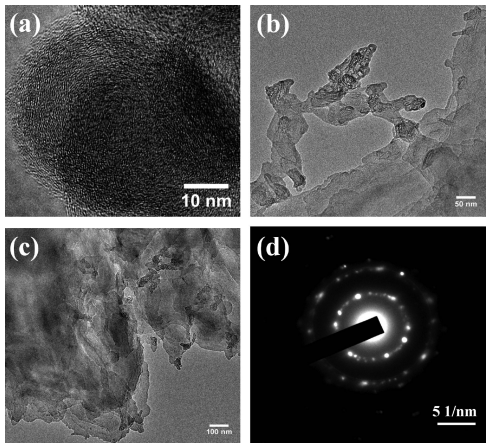

Figure 6. High-resolution TEM images. (a) Soot particle showing a discontinuous graphitic structure, (b) carbon nanotubes, (c) graphene-like sheet, and (d) SAED pattern showing the characteristic of a graphene-like sheet.

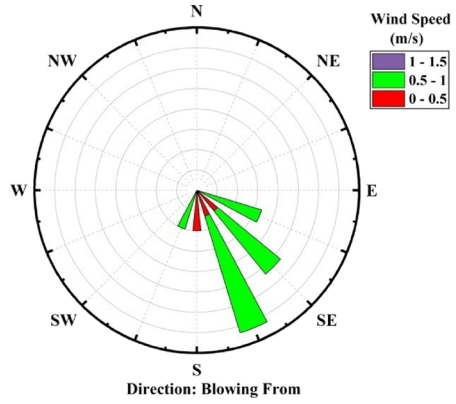

Figure 7. Wind rose showing the direction and speed of local wind toward the sampling site during the sampling period.

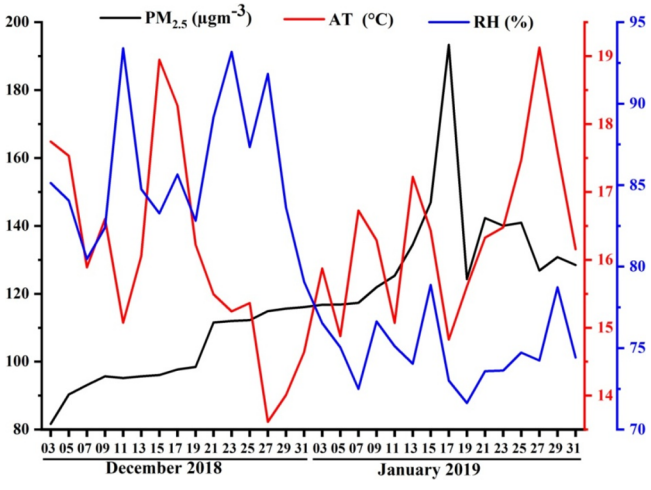

Figure 8. Variation of $PM_{2.5}$ mass concentrations, atmospheric temperature (°C), and relative humidity (%) in winter season (3rd Dec 2018 to 31st Jan 2019) in Jorhat area (Northeast India). The graph shows a gradual increase in $PM_{2.5}$ concentration from December to January. The sharp increase on 17th January might be due to the burning activity near the sampling site.

87.99%, max: 92%, and min: 64.70%), which increases the hygroscopic growth[60] of the particle, causing dry deposition.[61]

The moderately relative humidity was recorded during day time (average: 52.15%, max: 69.40%, and min: 39.50%) and winter days are shorter than night resulting less particle suspension time. Low wind speed increases PM concentration providing favorable conditions for particle formation showing a negative correlation.[58] The wind direction and long-range movement of air-mass affect the $PM_{2.5}$ pollution in a region.[20] In the study area of Jorhat, more pollutants are carried by the west wind from the Indo-Gangetic plain than the wind from other directions. The HYSPLIT air-mass back trajectories show that the air-masses were mainly from the west and southwest direction and moves through the Indo-Gangetic aerosol hot-spot region (Figure 1b); however, the wind rose shows that the wind direction was from the southeast direction (Figure 7). This contrasting difference could be because most of the air-mass moves towards the east and may be due to the presence of a mountain barrier in the north, east, and southeast directions; the air-mass returns to the sampling site in the southeast direction. Short-range and long-range back trajectories were observed, indicating the contribution of local aerosols and transboundary aerosols to the $PM_{2.5}$ in the study area.

4. CONCLUSIONS

Jorhat (Northeast India) experiences $PM_{2.5}$ far beyond the WHO permissible limit during winter season. The $PM_{2.5}$ in the region mainly consists of water-soluble inorganic ions, carbonaceous component, PAHs, and various trace elements. High winter loadings of $PM_{2.5}$ are contributed by various anthropogenic burning activities during winter in the Jorhat region, Northeast India, which further get aggravates due to the favorable weather condition of the region. Burning of biomass for heating and cooking and coal combustion in brick kilns and vehicles were the possible main contributors to $PM_{2.5}$ in the region. Meteorology plays a key role in high $PM_{2.5}$ pollution during winter high temperatures, low humidity, and low wind-speed accelerate $PM_{2.5}$ pollution in a region creating a favorable environment for aerosol formation. This implies the necessity of better regulatory actions especially during winter to minimize the impacts of $PM_{2.5}$ pollution.

AUTHOR INFORMATION

Corresponding Author

Binoy K Saikia − *Coal and Energy Group, Materials Science and Technology Division, CSIR-North East Institute of Science and Technology, Jorhat, Assam, India; Academy of Scientific and Innovative Research (AcSIR), Ghaziabad 201002, India;* orcid.org/0000-0002-3382-6218; Email: bksaikia@neist.res.in, bksaikia@gmail.com

Authors

Shahadev Rabha − *Coal and Energy Group, Materials Science and Technology Division, CSIR-North East Institute of Science and Technology, Jorhat, Assam, India; Academy of Scientific and Innovative Research (AcSIR), Ghaziabad 201002, India*

Gyanesh Kumar Singh − *Department of Civil Engineering, Indian Institute of Technology, Kanpur 208016, UP, India*

Tarun Gupta − *Department of Civil Engineering, Indian Institute of Technology, Kanpur 208016, UP, India*

Complete contact information is available at: https://pubs.acs.org/10.1021/acsearthspacechem.1c00037

Notes

The authors declare no competing financial interest.

■ ACKNOWLEDGMENTS

The director (CSIR-NEIST) is thankfully acknowledged by the authors for his permission to publish the paper. The fund was received from NCAP-COALESCE (GPP-325). The authors also acknowledge the NOAA Air Resources Laboratory (ARL) and the NASA FIRMS for the provision of the HYSPLIT model and fire data. The constructive and valuable comments received from the editor (Prof. V. Faye McNeill) and two anonymous reviewers to improve the revision are thankfully acknowledged.

■ REFERENCES

(1) Charlson, R. J.; Schwartz, S. E.; Hales, J. M.; Cess, R. D.; Coakley, J. A.; Hansen, J. E.; Hofmann, D. J. Climate Forcing by Anthropogenic Aerosols. *Science* **1992**, *255*, 423.

(2) Pöschl, U. Atmospheric Aerosols: Composition, Transformation, Climate and Health Effects. *Angew. Chem., Int. Ed.* **2005**, *44*, 7520−7540.

(3) Buseck, P. R.; Pósfai, M. Airborne minerals and related aerosol particles: Effects on climate and the environment. *Proc. Natl. Acad. Sci. U. S. A.* **1999**, *96*, 3372.

(4) Sekiguchi, M.; Nakajima, T.; Suzuki, K.; Kawamoto, K.; Higurashi, A.; Rosenfeld, D.; Sano, I.; Mukai, S. A study of the direct and indirect effects of aerosols using global satellite data sets of aerosol and cloud parameters. *J. Geophys. Res.: Atmos.* **2003**, *108* (), DOI: 10.1029/2002JD003359.

(5) Gawhane, R. D.; Rao, P. S. P.; Budhavant, K.; Meshram, D. C.; Safai, P. D. Anthropogenic fine aerosols dominate over the Pune region, Southwest India. *Meteorol. Atmos. Phys.* **2019**, *131*, 1497−1508.

(6) Streets, D. G.; Bond, T. C.; Carmichael, G. R.; Fernandes, S. D.; Fu, Q.; He, D.; Klimont, Z.; Nelson, S. M.; Tsai, N. Y.; Wang, M. Q.; Woo, J. H.; Yarber, K. F. An inventory of gaseous and primary aerosol emissions in Asia in the year 2000. *J. Geophys. Res.: Atmos.* **2003**, *108* (), DOI: 10.1029/2002JD003093.

(7) Requia, W. J.; Jhun, I.; Coull, B. A.; Koutrakis, P. Climate impact on ambient PM2.5 elemental concentration in the United States: A trend analysis over the last 30 years. *Environ. Int.* **2019**, *131*, 104888.

(8) Balakrishnan, K.; Dey, S.; Gupta, T.; Dhaliwal, R. S.; Brauer, M.; Cohen, A. J.; Stanaway, J. D.; Beig, G.; Joshi, T. K.; Aggarwal, A. N.; Sabde, Y.; Sadhu, H.; Frostad, J.; Causey, K.; Godwin, W.; Shukla, D. K.; Kumar, G. A.; Varghese, C. M.; Muraleedharan, P.; Agrawal, A.; Anjana, R. M.; Bhansali, A.; Bhardwaj, D.; Burkart, K.; Cercy, K.; Chakma, J. K.; Chowdhury, S.; Christopher, D. J.; Dutta, E.; Furtado, M.; Ghosh, S.; Ghoshal, A. G.; Glenn, S. D.; Guleria, R.; Gupta, R.; Jeemon, P.; Kant, R.; Kant, S.; Kaur, T.; Koul, P. A.; Krish, V.; Krishna, B.; Larson, S. L.; Madhipatla, K.; Mahesh, P. A.; Mohan, V.; Mukhopadhyay, S.; Mutreja, P.; Naik, N.; Nair, S.; Nguyen, G.; Odell, C. M.; Pandian, J. D.; Prabhakaran, D.; Prabhakaran, P.; Roy, A.; Salvi, S.; Sambandam, S.; Saraf, D.; Sharma, M.; Shrivastava, A.; Singh, V.; Tandon, N.; Thomas, N. J.; Torre, A.; Xavier, D.; Yadav, G.; Singh, S.; Shekhar, C.; Vos, T.; Dandona, R.; Reddy, K. S.; Lim, S. S.; Murray, C. J. L.; Venkatesh, S.; Dandona, L. The impact of air pollution on deaths, disease burden, and life expectancy across the states of India: the Global Burden of Disease Study 2017. *Lancet Planet. Health* **2019**, *3*, e26−e39.

(9) Saikia, J.; Roy, S.; Bordoloi, M.; Saikia, P.; Saikia, B. K. Atmospheric aerosols around three different types of coal-based industries: Emission parameters, cytotoxicity assay, and principal component analysis. *J. Aerosol Sci.* **2018**, *126*, 21−32.

(10) Rabha, S.; Saikia, J.; Subramanyam, K. S. V.; Hower, J. C.; Hood, M. M.; Khare, P.; Saikia, B. K. Geochemistry and Nano-mineralogy of Feed Coals and Their Coal Combustion Residues from Two Different Coal-Based Industries in Northeast India. *Energy Fuels* **2018**, *32*, 3697−3708.

(11) Pathak, B.; Subba, T.; Dahutia, P.; Bhuyan, P. K.; Moorthy, K. K.; Gogoi, M. M.; Babu, S. S.; Chutia, L.; Ajay, P.; Biswas, J.; Bharali, C.; Borgohain, A.; Dhar, P.; Guha, A.; De, B. K.; Banik, T.; Chakraborty, M.; Kundu, S. S.; Sudhakar, S.; Singh, S. B. Aerosol characteristics in north-east India using ARFINET spectral optical depth measurements. *Atmos. Environ.* **2016**, *125*, 461−473.

(12) Dahutia, P.; Pathak, B.; Bhuyan, P. K. Aerosols characteristics, trends and their climatic implications over Northeast India and adjoining South Asia. *Int. J. Climatol.* **2018**, *38*, 1234−1256.

(13) Bhuyan, P.; Barman, N.; Bora, J.; Daimari, R.; Deka, P.; Hoque, R. R. Attributes of aerosol bound water soluble ions and carbon, and their relationships with AOD over the Brahmaputra Valley. *Atmos. Environ.* **2016**, *142*, 194−209.

(14) Bhuyan, P.; Deka, P.; Prakash, A.; Balachandran, S.; Hoque, R. R. Chemical characterization and source apportionment of aerosol over mid Brahmaputra Valley, India. *Environ. Pollut.* **2018**, *234*, 997−1010.

(15) Tiwari, S.; Dumka, U. C.; Gautam, A. S.; Kaskaoutis, D. G.; Srivastava, A. K.; Bisht, D. S.; Chakrabarty, R. K.; Sumlin, B. J.; Solmon, F. Assessment of PM2.5 and PM10 over Guwahati in Brahmaputra River Valley: Temporal evolution, source apportionment and meteorological dependence. *Atmospheric Pollution Research* **2017**, *8*, 13−28.

(16) Deka, P.; Bhuyan, P.; Daimari, R.; Sarma, K. P.; Hoque, R. R. Metallic species in PM10 and source apportionment using PCA-MLR modeling over mid-Brahmaputra Valley. *Arabian Journal of Geosciences* **2016**, *9*, 335.

(17) Gogoi, P.; Chetry, N. Urban growth trend analysis of jorhat city. *Asian Acad. Res. J. Soc. Sci. Humanit.* **2016**, *3*, 270−284.

(18) Guttikunda, S. K.; Begum, B. A.; Wadud, Z. Particulate pollution from brick kiln clusters in the Greater Dhaka region, Bangladesh. *Air Qual., Atmos. Health* **2013**, *6*, 357−365.

(19) Guttikunda, S. K.; Calori, G. A GIS based emissions inventory at 1 km × 1 km spatial resolution for air pollution analysis in Delhi, India. *Atmos. Environ.* **2013**, *67*, 101−111.

(20) Pathak, B.; Bhuyan, P. K.; Gogoi, M.; Bhuyan, K. Seasonal heterogeneity in aerosol types over Dibrugarh-North-Eastern India. *Atmos. Environ.* **2012**, *47*, 307−315.

(21) Khare, P.; Baruah, B. P. Elemental characterization and source identification of PM2.5 using multivariate analysis at the suburban site of North-East India. *Atmos. Res.* **2010**, *98*, 148−162.

(22) Zhou, S.; Wang, Z.; Gao, R.; Xue, L.; Yuan, C.; Wang, T.; Gao, X.; Wang, X.; Nie, W.; Xu, Z.; Zhang, Q.; Wang, W. Formation of secondary organic carbon and long-range transport of carbonaceous aerosols at Mount Heng in South China. *Atmos. Environ.* **2012**, *63*, 203−212.

(23) Chakraborty, A.; Gupta, T. Chemical Characterization and Source Apportionment of Submicron (PM1) Aerosol in Kanpur Region, India. *Aerosol Air Qual. Res.* **2010**, *10*, 433−445.

(24) Mohseni Bandpi, A.; Eslami, A.; Shahsavani, A.; Khodagholi, F.; Aliaghaei, A.; Alinejad, A. Water-soluble and organic extracts of ambient PM2.5 in Tehran air: assessment of genotoxic effects on human lung epithelial cells (A549) by the Comet assay. *Toxin Rev.* **2017**, *36*, 116−124.

(25) Sharma, H.; Jain, V. K.; Khan, Z. H. Characterization and source identification of polycyclic aromatic hydrocarbons (PAHs) in the urban environment of Delhi. *Chemosphere* **2007**, *66*, 302−310.

(26) Saikia, J.; Khare, P.; Saikia, P.; Saikia, B. K. Polycyclic aromatic hydrocarbons (PAHs) around tea processing industries using high-sulfur coals. *Environ. Geochem. Health* **2017**, *39*, 1101−1116.

(27) Huang, D.; Hua, X.; Xiu, G.-L.; Zheng, Y.-J.; Yu, X.-Y.; Long, Y.-T. Secondary ion mass spectrometry: The application in the analysis of atmospheric particulate matter. *Anal. Chim. Acta* **2017**, *989*, 1−14.

(28) Rabha, S.; Saikia, B. K. An environmental evaluation of carbonaceous aerosols in PM10 at micro- and nano-scale levels reveals the formation of carbon nanodots. *Chemosphere* **2020**, *244*, 125519.

(29) Chow, J. C.; Wang, X.; Sumlin, B. J.; Gronstal, S. B.; Chen, L. W. A.; Trimble, D. L.; Watson, J. G.; Kohl, S. D.; Mayorga, S. R.; Riggio, G.; Hurbain, P. R.; Johnson, M.; Zimmermann, R. Optical Calibration and Equivalence of a Multiwavelength Thermal/Optical Carbon Analyzer. *Aerosol Air Qual. Res.* **2015**, *15*, 1145−1159.
(30) Kaul, D. S.; Gupta, T.; Tripathi, S. N.; Tare, V.; Collett, J. L. Secondary Organic Aerosol: A Comparison between Foggy and Nonfoggy Days. *Environ. Sci. Technol.* **2011**, *45*, 7307−7313.
(31) Kulshrestha, A.; Bisht, D. S.; Masih, J.; Massey, D.; Tiwari, S.; Taneja, A. Chemical characterization of water-soluble aerosols in different residential environments of semi aridregion of India. *J. Atmos. Chem.* **2009**, *62*, 121−138.
(32) Deshmukh, D. K.; Deb, M. K.; Tsai, Y. I.; Mkoma, S. L. Water Soluble Ions in PM2.5 and PM1 Aerosols in Durg City, Chhattisgarh, India. *Aerosol Air Qual. Res.* **2011**, *11*, 696−708.
(33) Tian, S.; Liu, Y.; Wang, J.; Wang, J.; Hou, L.; Lv, B.; Wang, X.; Zhao, X.; Yang, W.; Geng, C.; Han, B.; Bai, Z. Chemical Compositions and Source Analysis of PM2.5 during Autumn and Winter in a Heavily Polluted City in China. *Atmosphere* **2020**, *11*, 336.
(34) Ghosh, A.; Roy, A.; Chatterjee, A.; Das, S. K.; Ghosh, S. K.; Raha, S. Impact of Biomass Burning Plumes on the Size-Segregated Aerosol Chemistry over an Urban Atmosphere at Indo-Gangetic Plain. *Aerosol Air Qual. Res.* **2019**, *19*, 163−180.
(35) Chesselet, R.; Morelli, J.; Buat-Menard, P. Variations in ionic ratios between reference sea water and marine aerosols. *J. Geophys. Res.(1896-1977)* **1972**, *77*, 5116−5131.
(36) Chandra Mouli, P.; Venkata Mohan, S.; Jayarama Reddy, S. A study on major inorganic ion composition of atmospheric aerosols at Tirupati. *J. Hazard. Mater.* **2003**, *96*, 217−228.
(37) Bougiatioti, A.; Nenes, A.; Paraskevopoulou, D.; Fourtziou, L.; Stavroulas, I.; Liakakou, E.; Myriokefalitakis, S.; Daskalakis, N.; Weber, R.; Kanakidou, M.; Gerasopoulos, E.; Mihalopoulos, N. *Biomass burning and its effects on fine aerosol acidity, water content and nitrogen partitioning*; EGU General Assembly Conference Abstracts: 2017.
(38) Moravek, A.; Murphy, J. G.; Hrdina, A.; Lin, J. C.; Pennell, C.; Franchin, A.; Middlebrook, A. M.; Fibiger, D. L.; Womack, C. C.; McDuffie, E. E.; Martin, R.; Moore, K.; Baasandorj, M.; Brown, S. S. Wintertime spatial distribution of ammonia and its emission sources in the Great Salt Lake region. *Atmos. Chem. Phys.* **2019**, *19*, 15691−15709.
(39) Chen, Y.; Xie, S.-d.; Luo, B.; Zhai, C. Characteristics and Sources of Water-Soluble Ions in PM2.5 in the Sichuan Basin, China. *Atmosphere* **2019**, *10*, 78.
(40) Samburova, V.; Connolly, J.; Gyawali, M.; Yatavelli, R. L. N.; Watts, A. C.; Chakrabarty, R. K.; Zielinska, B.; Moosmüller, H.; Khlystov, A. Polycyclic aromatic hydrocarbons in biomass-burning emissions and their contribution to light absorption and aerosol toxicity. *Sci. Total Environ.* **2016**, *568*, 391−401.
(41) Mandalakis, M.; Gustafsson, Ö.; Alsberg, T.; Egebäck, A.-L.; Reddy, C. M.; Xu, L.; Klanova, J.; Holoubek, I.; Stephanou, E. G. Contribution of Biomass Burning to Atmospheric Polycyclic Aromatic Hydrocarbons at Three European Background Sites. *Environ. Sci. Technol.* **2005**, *39*, 2976−2982.
(42) Abdel-Shafy, H. I.; Mansour, M. S. M. A review on polycyclic aromatic hydrocarbons: Source, environmental impact, effect on human health and remediation. *Egypt. J. Pet.* **2016**, *25*, 107−123.
(43) Zhang, Y.; Tao, S. Global atmospheric emission inventory of polycyclic aromatic hydrocarbons (PAHs) for 2004. *Atmos. Environ.* **2009**, *43*, 812−819.
(44) Sandrini, S.; Fuzzi, S.; Piazzalunga, A.; Prati, P.; Bonasoni, P.; Cavalli, F.; Bove, M. C.; Calvello, M.; Cappelletti, D.; Colombi, C.; Contini, D.; de Gennaro, G.; Di Gilio, A.; Fermo, P.; Ferrero, L.; Gianelle, V.; Giugliano, M.; Ielpo, P.; Lonati, G.; Marinoni, A.; Massabò, D.; Molteni, U.; Moroni, B.; Pavese, G.; Perrino, C.; Perrone, M. G.; Perrone, M. R.; Putaud, J.-P.; Sargolini, T.; Vecchi, R.; Gilardoni, S. Spatial and seasonal variability of carbonaceous aerosol across Italy. *Atmos. Environ.* **2014**, *99*, 587−598.
(45) Zeng, T.; Wang, Y. Nationwide summer peaks of OC/EC ratios in the contiguous United States. *Atmos. Environ.* **2011**, *45*, 578−586.
(46) Cao, J. J.; Zhu, C. S.; Tie, X. X.; Geng, F. H.; Xu, H. M.; Ho, S. S. H.; Wang, G. H.; Han, Y. M.; Ho, K. F. Characteristics and sources of carbonaceous aerosols from Shanghai, China. *Atmos. Chem. Phys.* **2013**, *13*, 803−817.
(47) Zhang, R.; Tao, J.; Ho, K. F.; Shen, Z.; Wang, G.; Cao, J.; Liu, S.; Zhang, L.; Lee, S. C. Characterization of Atmospheric Organic and Elemental Carbon of PM2.5 in a Typical Semi-Arid Area of Northeastern China. *Aerosol Air Qual. Res.* **2012**, *12*, 792−802.
(48) Wang, Z.; Wang, T.; Guo, J.; Gao, R.; Xue, L.; Zhang, J.; Zhou, Y.; Zhou, X.; Zhang, Q.; Wang, W. Formation of secondary organic carbon and cloud impact on carbonaceous aerosols at Mount Tai, North China. *Atmos. Environ.* **2012**, *46*, 516−527.
(49) Liang, L.; Engling, G.; Cheng, Y.; Zhang, X.; Sun, J.; Xu, W.; Liu, C.; Zhang, G.; Xu, H.; Liu, X.; Ma, Q. Influence of High Relative Humidity on Secondary Organic Carbon: Observations at a Background Site in East China. *J. Meteorol. Res.* **2019**, *33*, 905−913.
(50) Englert, N. Fine particles and human health—a review of epidemiological studies. *Toxicol. Lett.* **2004**, *149*, 235−242.
(51) Fu, H.; Zhang, M.; Li, W.; Chen, J.; Wang, L.; Quan, X.; Wang, W. Morphology, composition and mixing state of individual carbonaceous aerosol in urban Shanghai. *Atmos. Chem. Phys.* **2012**, *12*, 693−707.
(52) Li, W. J.; Zhang, D. Z.; Shao, L. Y.; Zhou, S. Z.; Wang, W. X. Individual particle analysis of aerosols collected under haze and non-haze conditions at a high-elevation mountain site in the North China plain. *Atmos. Chem. Phys.* **2011**, *11*, 11733−11744.
(53) Li, W.; Shao, L. Transmission electron microscopy study of aerosol particles from the brown hazes in northern China. *J. Geophys. Res.: Atmos.* **2009**, *114* (), DOI: 10.1029/2008JD011285.
(54) Yang, Y.; Vance, M.; Tou, F.; Tiwari, A.; Liu, M.; Hochella, M. F. Nanoparticles in road dust from impervious urban surfaces: distribution, identification, and environmental implications. *Environ. Sci.: Nano* **2016**, *3*, 534−544.
(55) Murr, L. E.; Bang, J. J.; Esquivel, E. V.; Guerrero, P. A.; Lopez, D. A. Carbon Nanotubes, Nanocrystal Forms, and Complex Nanoparticle Aggregates in common fuel-gas combustion sources and the ambient air. *J. Nanopart. Res.* **2004**, *6*, 241−251.
(56) Tripathi, K. M.; Singh, A.; Bhati, A.; Sarkar, S.; Sonkar, S. K. Sustainable Feasibility of the Environmental Pollutant Soot to Few-Layer Photoluminescent Graphene Nanosheets for Multifunctional Applications. *ACS Sustainable Chem. Eng.* **2016**, *4*, 6399−6408.
(57) Murr, L. E.; Bang, J. J. Electron microscope comparisons of fine and ultra-fine carbonaceous and non-carbonaceous, airborne particulates. *Atmos. Environ.* **2003**, *37*, 4795−4806.
(58) Dawson, J. P.; Adams, P. J.; Pandis, S. N. Sensitivity of $PM_{2.5}$ to climate in the Eastern US: a modeling case study. *Atmos. Chem. Phys.* **2007**, *7*, 4295−4309.
(59) Yang, Q.; Yuan, Q.; Li, T.; Shen, H.; Zhang, L. The Relationships between PM2.5 and Meteorological Factors in China: Seasonal and Regional Variations. *Int. J. Environ. Res. Public Health* **2017**, *14*, 1510.
(60) Liu, P. F.; Zhao, C. S.; Göbel, T.; Hallbauer, E.; Nowak, A.; Ran, L.; Xu, W. Y.; Deng, Z. Z.; Ma, N.; Mildenberger, K.; Henning, S.; Stratmann, F.; Wiedensohler, A. Hygroscopic properties of aerosol particles at high relative humidity and their diurnal variations in the North China Plain. *Atmos. Chem. Phys.* **2011**, *11*, 3479−3494.
(61) Wang, J.; Ogawa, S. Effects of Meteorological Conditions on PM2.5 Concentrations in Nagasaki, Japan. *Int. J. Environ. Res. Public Health* **2015**, *12*, 9089.

https://doi.org/10.1021/acsearthspacechem.1c00037
ACS Earth Space Chem. 2021, 5, 1686−1694